Research Article

Patricio La Delfa*, Michel Hecquet, and Frederic Gillon

Inverse approach for concentrated winding surface permanent magnet synchronous machines noiseless design

https://doi.org/10.1515/phys-2019-0066
Received May 15, 2019; accepted Jul 27, 2019

Abstract: The electromagnetic noise generated by the Maxwell radial pressure is a well-known consequence. In this paper, we present an analytical tool that allows air gap spatio-temporal pressures to be obtained from the radial flux density created by surface permanent magnet synchronous machines with concentrated winding (SPMSM). This tool based on winding function, a global air-gap permeance analytical model and total magnetomotive force product, determines the analytical air-gap spatio temporal and spectral radial pressure. We will see step-by-step their impacts in generating noise process. Also two predictive methods will be presented to determine the origin of the lows radial pressure orders noise sources. The interest lies in keeping results very quickly and appropriate in order to identify the low order electromagnetic noise origin. Then through an inverse approach using an iterative loop a new winding function is proposed in order to minimize radial force low order previously identified and chosen.

Keywords: Low order, spatio-temporal, radial pressure, permeance, inverse approach

PACS: 03.50.De, 41.20.-q, 77.65.Fs, 02.30.Zz

Nomenclature

$\sigma(t,a_s)$	Spatio-temporal radial pressure
$\wedge(t,a_s)$	Global permeance
a_s	Mecanical space angle
$[I_{ph}^t]$	Three-phase sinusoidal current matrix
$[N_{ph}^{a_s}]$	Three-phase winding and distribution function matrix
$B(t,a_s)$	Spatio-temporal flux density
MMF	Total magnetomotive force
MMFr	Rotor magnetomotive force
MMFs	Stator magnetomotive force
t	Temporal space

1 Introduction

In order to preserve primary energy and reduce greenhouse emissions the electrical motors have been developed and significantly improved. In addition the use of magnets and concentrated winding contributed to increase the efficiency and power density of SPMSM in transport, energy production and industrial automation applications. It is essential to take into account both the electrical characteristics when designing electrical machines and the electromagnetic acoustic noise radiated. This source of audible noise arises when Maxwell pressures induce dynamic deflections of the external structure (stator or rotor), which then propagate in the ambient air as acoustic waves [1, 2]. Many references provide analytical relations in order to evaluate this radial pressure , the interaction between the slotting and the magnetomotive force (MMF) or the saturation effect force [2–5].

In this paper, the origin of the spatio-temporal radial pressure is investigated taking into account analytical models considering the total magnetomotive force (stator/rotor), the global permeance, winding and distribution function. From then on, we introduce the functional organization calculation tool. In addition we will identify and analyse the lowest space order of the radial air-gap pressure (Maxwell pressure) which represents a potential risk of noise pollution, i.e. the harmonics specific to the magnet, and the teeth and their interactions. Also the contribution of each air-gap spatio-temporal flux density $B(t,a_s)$

***Corresponding Author: Patricio La Delfa:** Univ. Lille, Arts et Metiers ParisTech, Centrale Lille, HEI, EA 2697 - L2EP -Laboratoire d'Electrotechnique et d'Electronique de Puissance, F-59000 Lille, France; Email: patricio.la-delfa@univ-lille.fr
Michel Hecquet, Frederic Gillon: Univ. Lille, Arts et Metiers ParisTech, Centrale Lille, HEI, EA 2697 - L2EP -Laboratoire d'Electrotechnique et d'Electronique de Puissance, F-59000 Lille, France

harmonic to identify the origin of each harmonic spatio-temporal radial pressure $\sigma(t,a_s)$, is not easy. In order to identify and understand the origin of the low air gap radial pressure, we have used two analytical predictive methodology approaches. The first implements the air gap flux density considering the total MMF by global permeance $\wedge(t,a_s)$ product [6]. The second one given by [7] used the convolution product based on two-dimensional Direct Fourier Transform, (2D-DFT) of radial flux density and its convolution with itself. At last, an iterative loop considering experimental design will be defined depending constrains and different factors. The main objective of the investigations is to propose a new winding function design which minimizes the lowest air gap radial pressure previously identified and chosen.

2 Analytical calculation tool

The Figure 1 shows our direct approach to calculate the flux density in time and space. Its enables the different physical aspects to be obtained step-by-step, from the sinusoidal current matrix $[I_{ph}^t]$ set up to the Maxwell radial pressure $\sigma(t,a_s)$. The analytical model takes into account the global permeance $\wedge(a)$ given by [6], winding and distribution function $[N_{ph}^{\alpha_s}]$ matrix and the total magnetomotive force MMF to obtain the spatio-temporal flux density $B(t,a_s)$ and spatio-temporal radial pressure.

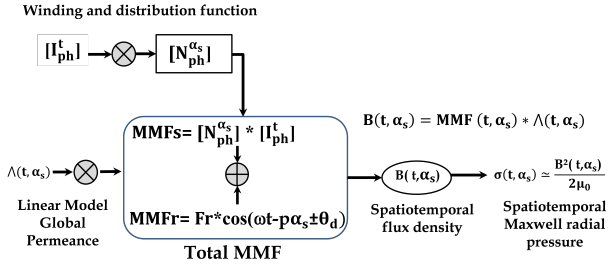

Figure 1: Functional organization of radial pressure analytical tool

3 Scope of the work

In this study, we consider modular SPMSM [8], composed of ten poles and twelve slots provided with concentrated winding (CW) as show Figure 2a determined according the star of slots method, [9]. We appreciate the different elementary coils implanted which constitute the double winding implanted into the diametrically opposite slots. The winding function matrix N_{ph}^s indicates the number of elementary coils and the winding direction for the three phases that constitute the machine concentrated winding.

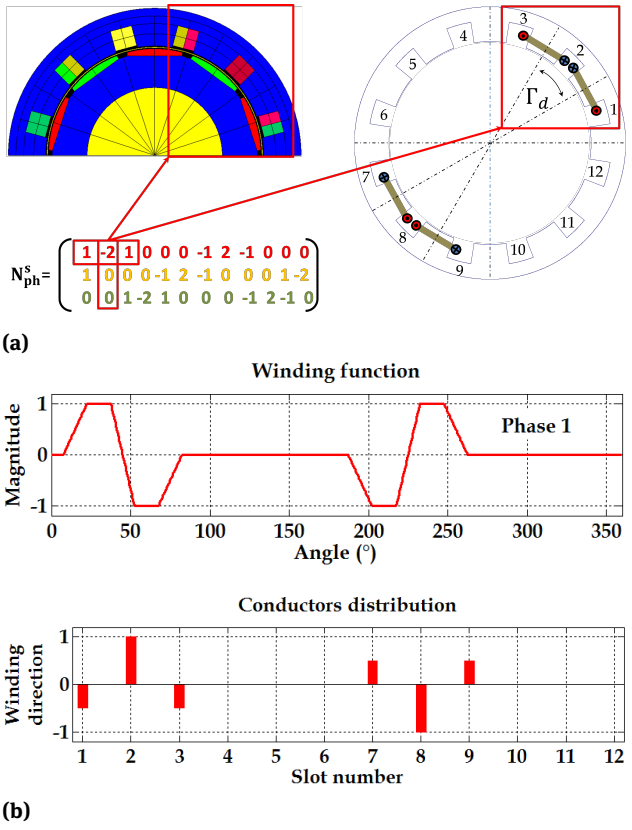

Figure 2: SPMSM description and winding function

Figure 2b shows the winding function and distribution of conductors in the mechanical space.The tool considers the opening slots and the winding direction of the elementary coils implanted in the stator slots. However several modular or asymmetric machines were also tested. Indeed, our tool enables implementation of a distributed winding regardless of the number of slots.

4 Electromagnetic field calculation

The air-gap flux density (1) is given considering the total MMF by global permeance $\Lambda\,(t,\ \alpha_s)$ product with α_s which represents the stator angle reference. The total MMF is composed of $f_{mm}^s\,(t,\ \alpha_s)$ and $f_{mm}^r\,(t,\ \alpha_s)$ respectively relative MMF stator (2) and rotor (3). From the air-gap radial flux density $B\,(t,\alpha_s)$ (1), the air-gap radial Maxwell pressure $\sigma_n\,(t,\alpha_s)$ can be calculated (4) in N/m^2. In this paper, only the radial values are considered, indeed radial

and tangential for $B(t, \alpha_s)$ and $\sigma_n(t, \alpha_s)$ harmonics appear at the same carrier frequency. Only their magnitude differs.We assumes that the magnetic circuit is unsaturated and that the permeability of the material is higher compared to that of the air. Also, in [10] it is shows the tangential flux density effect increases around twenty percent the radiated noise emission.

$$B(t, \alpha_s) = \Lambda(t, \alpha_s) * \left[f^s_{mm}(t, \alpha_s) + f^r_{mm}(t, \alpha_s)\right] = \Lambda(t, \alpha_s) * f_{mm}(t, \alpha_s) \quad (1)$$

$$f^s_{mm}(t, \alpha_s) = \sum_{ph=1}^{3} N^s_{ph}(\alpha_s) . I^s_{ph}(t) \quad (2)$$

$$f^r_{mm}(t, \alpha_s) = fr * cos(\omega t - p\alpha_s \pm \theta_d) \quad (3)$$

$$\sigma_n(t, \alpha_s) = \frac{\left(\Lambda(t, \alpha_s) . \left[f^s_{mm}(t, \alpha_s) + f^r_{mm}(t, \alpha_s)\right]\right)^2}{2\mu_0} \quad (4)$$

At this stage we propose to describe our analytical tool for determining the physical quantities involved and their associated spectrums, thus offering the possibility of understanding phenomenon's and analysis step by step.

4.1 Permeance model

The global air gap permeance analytical model defined by [6] is constituted by four term with Λ_0, the mean value (constant value linked to air gap thickness); Λ_s, the effect of the stator slots (terms series depending of stator slots); Λ_r, the effect of the rotor from the magnet shape (terms series depending of rotor slots) and Λ_{sr}, the mutual effect stator and rotor (5).

$$\Lambda(t, \alpha_s) = \Lambda_0 + \Lambda_s(\alpha_s) + \Lambda_r(t, \alpha_s) + \Lambda_{sr}(t, \alpha_s) \quad (5)$$

The Figure 3a shows the spatio-temporal global air gap permeance. All effects of the global air gap permeance, i.e. all terms defined in relation (5), are illustrated. Additionally it shows progress in time following the rotational movement of the rotor. The top view combines the effects linked to the stator, rotor and mutal effect. The space axis revels a maximal value variation which introduces the spatio-temporal order [2,2] visible in Figure 3b. The harmonics [r,f] represents the number of waves or spatial order 'r' and the frequency 'f'. It is identify as result of mutual effect stator/rotor. Also we observe the global air gap permeance FFT, with [−12,0], [12,0], [0,0] harmonics respectively linked the stator teeth and the permeance mean

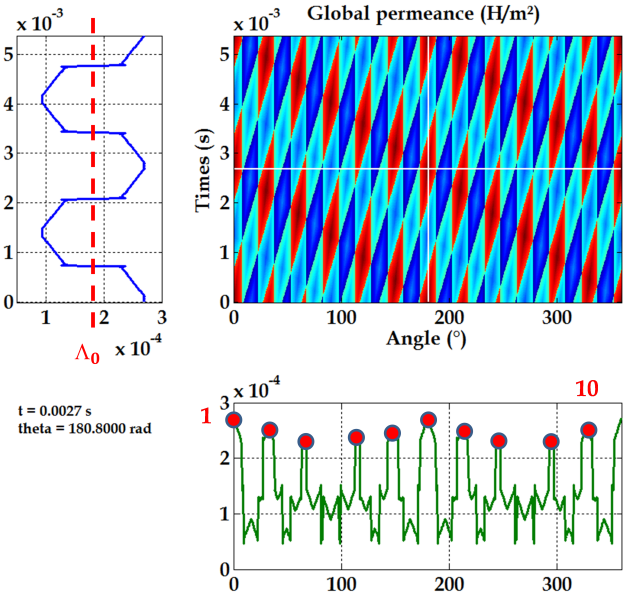

(a) Global permeance

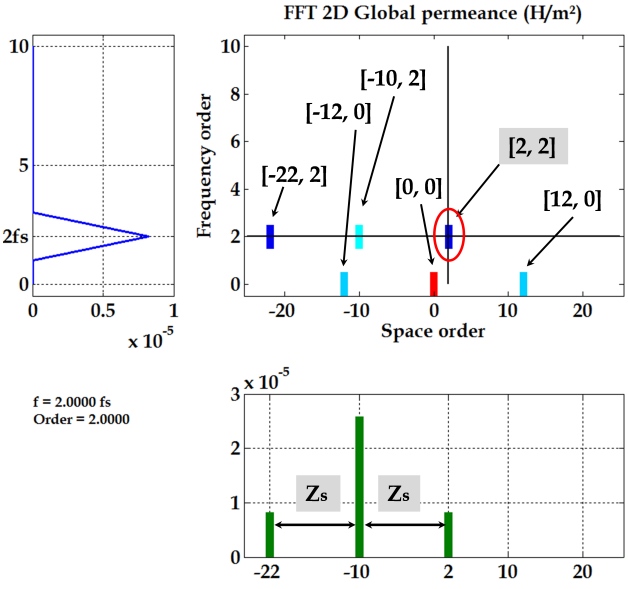

(b) FFT 2D Global permeance

Figure 3: Spatio-temporal and spectral global air gap permeance

value. The number of poles pairs p distributed all along the stator space and the iron length is identify as harmonics [−10,0] due to rotor magnets.

Throught Figure 3b analysis we can confirm the mutual stator/rotor effect generates harmonics [2,2], [22,2] spaced one step egal to the number of slots Z_s around the pole pair p harmonic [10,2]. The orders genereted by the three first effects are now identifed and resumed in Table 1.

To conclude on this part, several studies to determine the gap permeance were conducted for example, the

Table 1: Permeance effect orders

Effects	Permeance orders results	Orders	frequency
Λ_0	[0,0]	0	0
Λ_s	[±12, 0];[0,0]	$k_s Z_s$;k_s ={0,1,2,3,...}	0
Λ_r	[±10,0]; [0,0]	k_r2p ;k_r ={0,1,2,3,...}	$k_r\ 2f_s$
$\Lambda_s + \Lambda_r$	[±12,0];[0,0];[±10,0]	$k_s Z_s$ + k_r2p	$k_r\ 2f_s$
$\Lambda_s \Lambda_r$	[±12,0];[0,0];[±10,0];*[2,2]*	$k_s\ Z_s \pm k_r$ 2p	$\pm\ k_s\ 2f_s$

Table 2: Space and frequency MMF formulation

	Space order	Frequency order
FMMs	(1±2q k); k={0,1,2,3...}	*fs*
FMMr	(2k±1).p; k={0,1,2,3...}	(2k±1).*fs*

analytical complex model [11] and local constant permeance [12].

4.2 Magnetomotive force model

The total magnetomotive force (MMF) is investigate considering the stator magnetomotive force (MMFs) (2) and rotor magnetomotive force (MMFr) (3). The MMFs model considers the matrix winding function N^s_{ph} previously presented and the 'q' phase's matrix sinus wave current injected. It takes account of the space and time discretization impact according to Shannon Theorem conditions. The MMFr injected is also considered as a sinus wave linked to the shape our magnets. Although the tool offers the possibility of injecting specifics harmonics to take into account the real shape and magnetization.

The MMFr spectral analysis reveals, the number of rotor poles pair p harmonic [−5,1] Figure 4a. The total MMF, Figure 4b, makes evident the MMFs linked to the winding function and the sinus wave supply generate the main harmonic [7,1] and [−5,1] too. These two aims harmonics are respectively a consequence of rotor poles pair p and the combination of [0,0] permeance mean value order, considering the relation (5), Table 1, and [7,1] order genereded by MMFs. The latter which represents the fundamental electromagnetic torque. Note the Table 2 summarizes the relations to determine the total MMF order's and frequencies.

4.3 The air-gap radial flux density model

Considering the relation (1), with the global permeance and the total MMF, we can calculate the radial flux density.

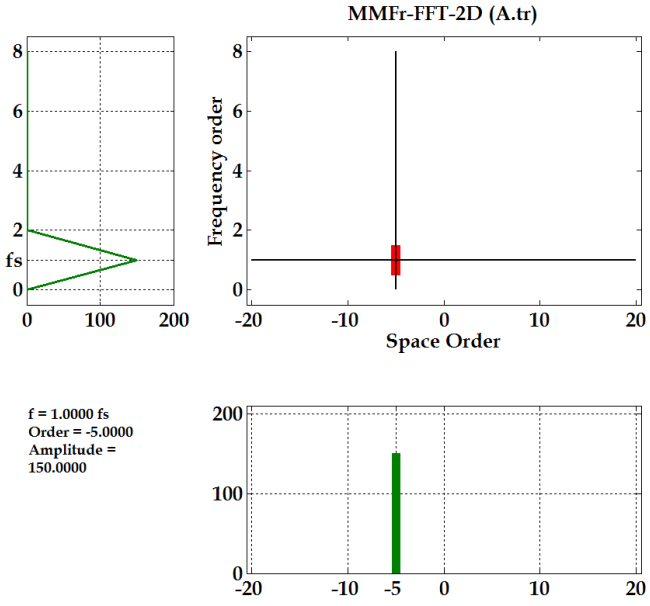

(a) Rotor magnetomotive force

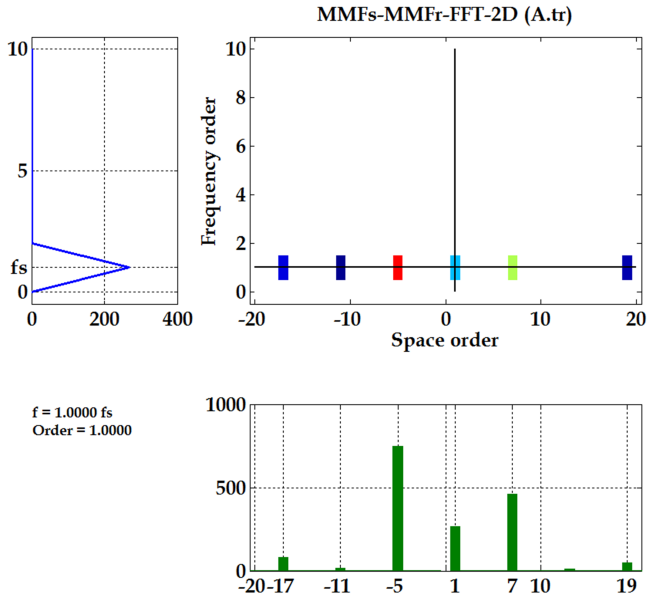

(b) Total magnetomotive force

Figure 4: Total magnetomotive force MMF

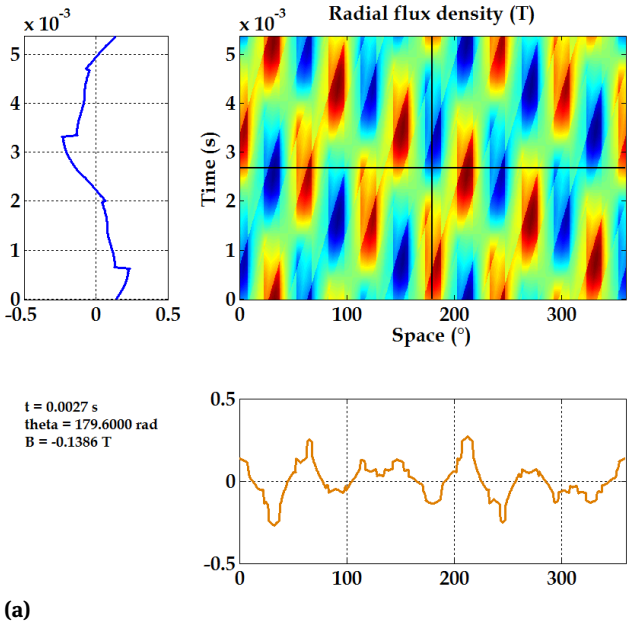

(a)

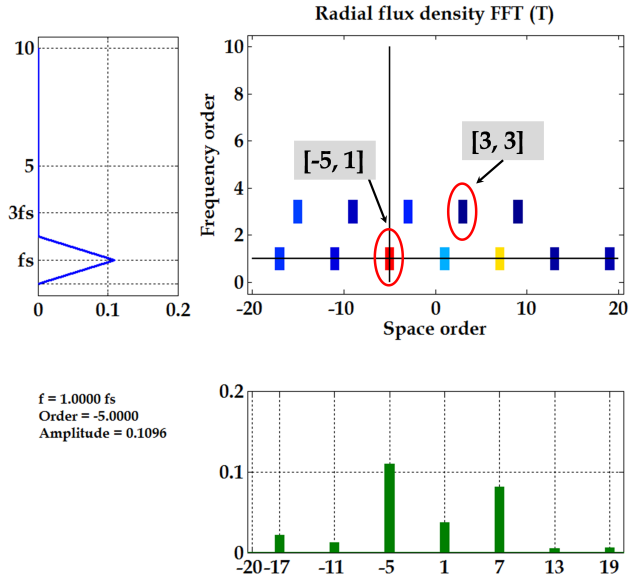

(b)

Figure 5: Spatio-temporal and spectral air gap radial flux density

Figure 5a-b illustrates respectively the spatio-temporal and 2D-FFT radial flux density : Figure 5a, the representation versus space and time (t : one electrical period, a_s : 0 to 360°); Figure 5b the 2D-FFT gives the space and frequency orders. We find the harmonics [–5, 1] and [7, 1] previously mentioned.

Also we observe the [3,3] order, the latter considering the relation (1) and the mathematical rules relating to the product of functions, "cosine, sinus" is related to the [2,2] permeance and the [1,1] MMF orders.

4.4 Air-gap radial pressure model

From the analytical air-gap radial flux density versus time and space, the air-gap radial Maxwell pressures σ (t, a_s) (N/m^2) can be calculated by the equation (4). Then, the spatial (or circumferential) and frequency orders can be defined with 2D Fast Fourier Transform (FFT) versus time and space.

The Figure 6a-b compares respectively the airgap radial pressure 2D-FFT obtained by finite element method (FE) and the analytical tool previously presented. The lowest order 2 at 2*fs* appears through the FE simulation and tool's results. Many even orders spaced by a step equal to $Z_s/2$ at 2k*fs* appear with k={0,1,2,3...}. We find the orders linked to rotor poles and stator slots. Moreever the FE simulation validates our analytical model.

For double-layer concentrated winding the spatial and frequency harmonic content is quite rich [13, 14]. The main harmonic [–10, 2] of radial pressure has the highest magnitude as it is linked to the number of poles. The spatial order 2 to 2f, which is a characteristic of this winding type, is observed linked to the Greatest Common Divider GCD (Zs, 2p) [13, 15]. The spatial order 0 (0f – 6f and 12f) exits and corresponds to the breathing mode for the electrical machines [15, 16]. Also the spatial and frequency orders [r, f] of these motors can be summarised as [17] in (6). With n, m, k= 0, 1, 2,... and p, Z_s and f_s are respectively the number of poles, the number of the stator slots and the electrical frequency.

$$[r, f] = [2np \pm 6mp \pm kZ_s; 2nf_s] \tag{6}$$

The main harmonic of the pressure is obtained when n = 1 and m = k = 0: r = –10 at $2f_s$, Figure 6a. When n = m = 0 and k = 1, the spatial order is –12 and 12 at $0f_s$ as we can see in Figure 6b.

The low spatial order (r = 2) at $2f_s$ is obtained by the interaction between magnet (2np) and teeth effects (kZ_s) : n = 1 and k = 1 (m = 0). Also, for the breathing mode (r = 0) at for example $6f_s$, this case is obtained by the magnet (2np) and stator field (6mp) effects: n = 3 and m = 1 (k = 0) and for $12f_s$ with n = 6 and k = 5 (m = 0), i.e. magnet and teeth effects. This harmonic linked to the interaction between teeth and magnet [0, 12] is very important point for the noise of the "classical machine": for example the PMSM with 8 poles and 48 teeth [17]. In our case, we have several low spatial orders (0, –2 and 2) for different frequency.

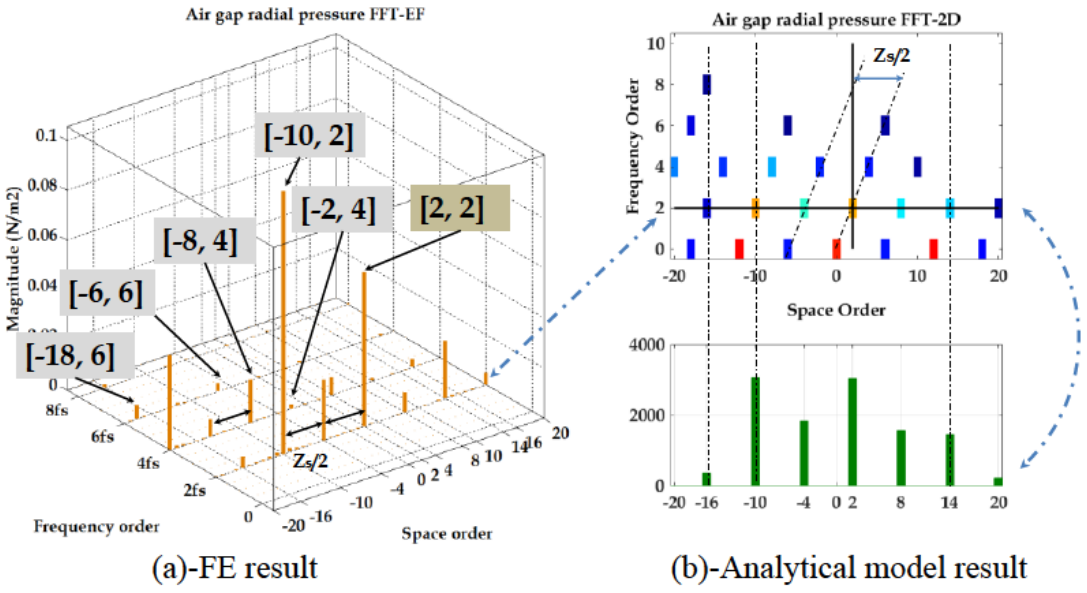

Figure 6: FFT-2D Air gap radial pressure

5 Predictive methodology approaches

Two predictive methods have been detailed in order to determine the origin of the low radial pressure orders linked to the noise sources. The interest lies in keeping the results very quick and appropriate in order to identify the low order electromagnetic noise origin

5.1 Analytical predictive methodology approach

Based on [2, 3] works, this predictive approach identifies all the space orders and frequencies of the air-gap Maxwell pressure harmonics. It also tracks the origin of the lowest space orders, i.e. combined interactions between the armature (winding), magnets and slotting effects (permeance), and its own interactions too [13].

The relation created from (4) is given in (7) where r,f; υ, f_s; $\mu p, f_s$; are respectively space and frequency order air-gap radial pressure, armature effect (winding) and magnet effect. We observe three principal groups, the first linked to the slotting effect and MMFs, the second linked to the slotting effect and MMFr. The third comes out of the slotting effect and MMF. Note all air-gap radial pressure orders are determined considering amplitude equal to unit and happen regardless.

$$\sigma_n^{r,f} = \underbrace{\frac{1}{2\mu_o}\left(\Lambda^{r,f_\Lambda}\right)^2 \cdot \left(f_s^{\upsilon,f_s}\right)^2}_{first} + \underbrace{\frac{1}{2\mu_o}\left(\Lambda^{r,f_\Lambda}\right)^2 \cdot \left(f_r^{\mu p,f_s}\right)^2}_{second} + \underbrace{\frac{1}{\mu_o}\left(\Lambda^{r,f_\Lambda}\right)^2 \cdot f_s^{\upsilon,f_s} \cdot f_r^{\mu p,f_s}}_{third} \tag{7}$$

Taking into account the Table 3, it comes out of the lowest order [2,2] origin identified. We notice many armature harmonics have a consistent impact, indeed the armature effect is found under the three subharmonics groups. To conclude this part, the air-gap pressure low order 2 at *2fs* represents the total effect given by the predictive approach, i.e. linked armature order, magnets-permeance, magnets-armature and magnet-permeance-armature interactions.

5.2 Convolution predictive methology approch

In order to compare our predictive methodology approach, results in Table 3, we used the convolution approach. This approach as given in [7], is based the two-dimensional Direct Fourier Transform (2D-DFT) of the air-gap radial flux density and its convolution with itself (7).

$$\sigma_{2DFT}(r,f) = \frac{1}{2\mu_0} * \left[B_{2D-DFT}(k_1,f_1) * B_{2D-DFT}(k_2,f_2)\right] \tag{8}$$

This approach imposes the radial flux density from FE simulation or analytical matrix. The FE matrix is characterized

Table 3: Analytical orders 2 at 2*fs* radial pressure results

Order 2 at 2fs		Harmonics origin due to effects of:
Subharmonics	Group	Armature
2υ	first	H_υ 1
$(\upsilon_2 \pm \upsilon 1)$	1	**H_υ 5, H_υ 7**, H_υ17, H_υ19,...
		Interaction-Magnets-Permeance
$(\mu_1 \pm \mu_{th}).p \pm k.Z_s$	second	H_μ 1, H_μ 3 ; (k = 1)
		Armature-Magnets
$(\mu \pm \upsilon).p$	third	(**H_μ 1 (*p)** , **H_υ 7**); (H_μ 3 (*p) , H_υ 19);
		Magnets-Permeance-Armature-
$(\mu \pm \upsilon).p \pm k_s Z_s$; k={0,1,3,...}	third	**H_υ 5** , **H_μ 3** (k=1)

Table 4: Aim convolution predictive approach results

Order pressure		Order flux density				Radial pressure	
r	f/fs	k_1	k_2	f_1	f_2	Amp (N/mm^2)	Phase (°)
2	2	1	1	fs	fs	1505.33	−32.60
		−3	5	3fs	fs	3637.88	−52.36
		−5	**7**	fs	fs	**31790.37**	**1.06**
		−15	17	3fs	fs	3198.91	49.08
		−17	19	fs	fs	1849.00	54.93

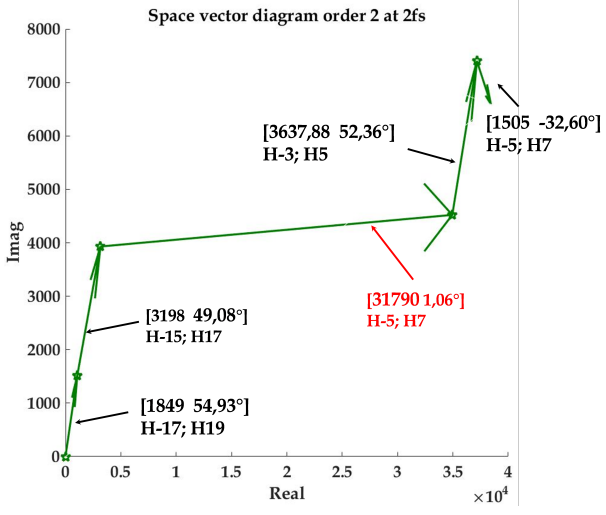

Figure 7: Space vector diagram air gap radial pressure by convolution product

by an important simulating and computing time considering all of the orders. However this approach offers the possibility to determine the amplitude and the phase of the radial pressure for each other low order and justify the order 2. Table 4 gives the most important magnitude harmonics and the frequencies that are at the origin of the order 2. Principally we find H = −5 and H = 7 with important magnitude, (Ten times' higher than the others orders). These harmonics have been previously identified Table 3 as magnet, armature, permeance and own interaction effects. One can confirm these aim radial flux density harmonics are at the origin of order 2 at 2*fs*.

The space vector diagram in Figure 7 illustrates the main radial flux density complex vectors harmonics at the origin of radial pressure order 2 at 2*fs* in the air gap.

In view of previous predictive and analytical tool results, the armature comes out of a main impact in low order production. Save for later inverse methodology winding determination minimizing low order can be done.

6 Inverse methodology

In order to resolve the inverse problem the main objective involves determing the winding function which cancels or decrease magnitude the previously low order magnitude [2,2]. The number of layers and the direction of winding to be installed can then be determined. Also the solution S requires two constraints, equality and inequality to be defined in order to respect the feasibility domain, (9), (10). The inverse problem linked to the design of noiseless machine can be assimilated as a constraint single objective

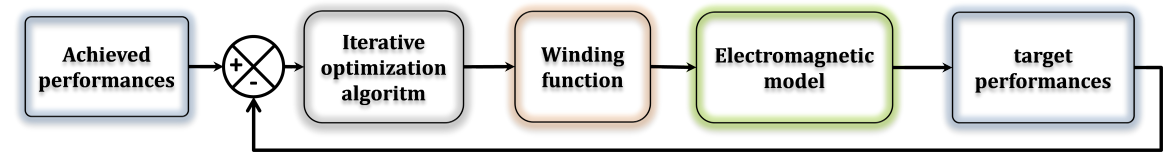

(a)

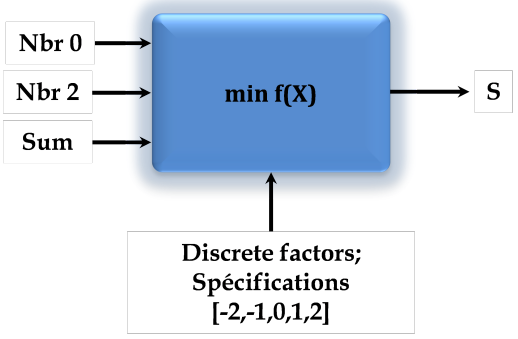

(b)

Figure 8: Inverse problem description

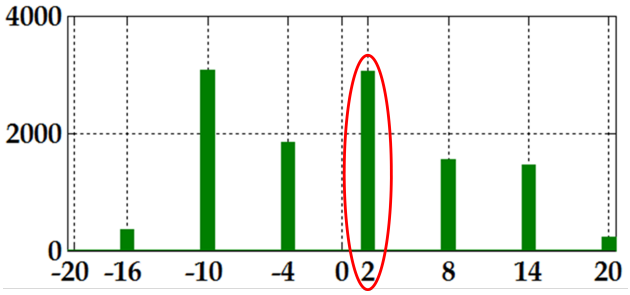

(a) initial radial pressure FFT

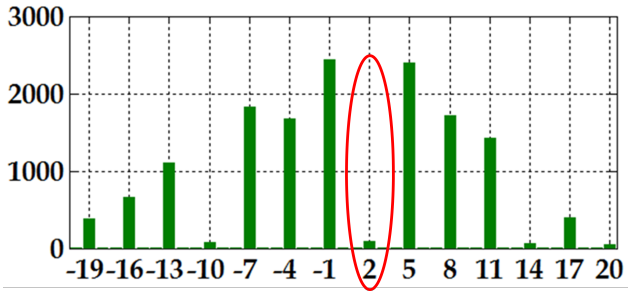

(b) optimised radial pressure FFT

-1	2	-1	0	0	0	1	-2	1	0	0	0
1	0	0	0	-1	2	-1	0	0	0	1	-2
0	0	1	-2	1	0	0	0	-1	2	-1	0

(c) initial winding function

-1	-1	1	0	0	0	0	0	1	-1	-1	2
1	-1	-1	2	-1	-1	1	0	0	0	0	0
0	0	0	0	1	-1	-1	2	-1	-1	1	0

(d) optimised winding function

Figure 9: Optimization air-gap radial pressure and winding function comparison

function (11).

$$g_k(X) \leq 0 \quad k = 1, \ldots, n \tag{9}$$

$$h_k(X) = 0 \quad k = 1, \ldots, m \tag{10}$$

$$\min f(X) = 0 \quad X = \{x_1, x_2, \ldots, x_i\} \in S \tag{11}$$

The inverse problem is shown in Figure 8a. We find parameters of constraints and factors linked to the concentrated winding. Indeed 0, ±1, or ±2 elementary winding may be implanted in the stator according to the winding function. According to the number and the five level filling slots, 5^{12} winding solutions are conceivable. The constraints imposed on our optimization tool named Sophemis © depend on the number of elementary double 'N_{br2}' or zero 'N_{br0}' elementary coils to be implanted, Figure 8b. Consequently, the simple elementary coils result from terms equal to zero. This is the reason for the requirement that the total 'Sum' of all the terms that make up the winding function is zero, Figure 9c. Note the minimal value is equal to unit for N_{br2} and N_{br0}. In Figure 9 respectively initial and optimized according to the air gap radial pres-

sure low orders [2,2], only for 2 *fs* and the winding function matrix N_{ph}^{s} are illustrated.

The comparison shows a smaller magnitude for the low order [2, 2] although the spectrum is richer. We conclude that the single objective function "minf(X)" is globally achieved. Moreover it is possible through an optimization loop to determine the electrical machine noiseless winding function.

Based on a sample of the results of the solutions it is necessary to follow the investigations through a more exhaustive algorithm (NSGA II) for example.

7 Conclusion

An analytical tool which enables the air-gap spatio-temporal pressures from the radial flux density to be obtained through the MMF winding function and the global permeance has been described. The spectral analysis results show low space orders generated in the air gap.

In addition, a predictive methodology allowed the origins of the noisy lowest air gap radial pressure order to be identified. The latter linked to the winding function trough the stator magnetomotive force and the permeance stator-rotor mutual term leads to a reduction in the low order magnitude previously identified. Finally, an optimization loop with a single objective and discrete parameters has been used to determine a winding function minimizing the magnitude [2, 2] completely identified.

References

[1] Timar P. L., Noise and vibration of electrical machine, - manual 1^{st} edition, Elsevier, 1989.

[2] Gieras J. F., Wang C., Cho Lai J., Noise of polyphase Electric Motors,-manual 1^{st} edition, CRC press, Taylor& Francis, 1994.

[3] Huang S., Aydin M., Lipo T.A., Electromagnetic vibration and noise assessment for surface mounted PM machines, In: Power Engineering Society Summer Meeting, Conference Proceedings, IEEE, 2001, 1417-1426.

[4] Besnerais J.Le, Reduction of magnetic noise in PWM-supplied induction machines: low-noise design rules and multi-objective optimisation, PhD thesis, Ecole Centrale de Lille, Lille, France, 2008.

[5] Lecointe J.P., Cassoret B., Brudny J.F., Distinction of Toothing and Saturation effects on magnetic noise induction motors, Progress In Electromagnetics Research., 2011,112,125–137.

[6] Cassoret B., Corton R., Roger D., Brudny JF., Magnetic noise reduction of induction machines. IEEE Transactions on power electronics, 18.2, 2003, 570-579.

[7] Van Der Giet M., and et al, A novel approach to estimate harmonic force excitation for noise diagnosis of electrical machines, ICS Newsletter, 16.1, 2009, 11-17.

[8] Islam R., Husain I., Analytical model for predicting noise and vibration in permanent-magnet synchronous motors, IEEE Transactions on industry applications, 46.6, 2010, 2346-2354.

[9] Cros J., Viarouge P., Synthesis of high performance PM motors with concentrated windings, IEEE transactions on energy conversion, 17.2, 2002, 248-253.

[10] Devillers E., and et al, An improved 2-D subdomain model of squirrel-cage induction machine including winding and slotting harmonics at steady state, IEEE Transactions on Magnetics, 54.2, 2018, 1-12.

[11] Fakam M., and et al, Design and magnetic noise reduction of the surface permanent magnet synchronous machine using complex air-gap permeance, IEEE Transactions on Magnetics, 51.4, 2015, 1-9.

[12] Bracikowski N., and et al, Multiphysics modeling of a permanent magnet synchronous machine by using lumped models, IEEE Transactions on Industrial Electronics, 59.6, 2011, 2426-2437.

[13] La Delfa P., and et al, Low space order analysis of radial pressure in SPMSM with analytical and convolution approaches, IEEE Transactions on Magnetics 52.11, 2016, 1-7.

[14] Tollance T., and et al, Design of Low Power Motors with a Good Compromise Between Ripple Torque and Radial Forces, XIII International Conference on Electrical Machines (ICEM), IEEE, 2018.

[15] Le Besnerais J., Vibroacoustic analysis of radial and tangential air-gap magnetic forces in permanent magnet synchronous machines, IEEE Transactions on Magnetics, 51.6, 2015, 1-9.

[16] Hofmann A., et al., The breathing mode-shape 0: Is it the main acoustic issue in the PMSMs of today's electric vehicles, 17th International Conference on Electrical Machines and Systems (ICEMS), IEEE, 2014.

[17] Andersson A., Torbjörn T., Electrical machine acoustic noise reduction based on rotor surface modifications, IEEE Energy Conversion Congress and Exposition (ECCE), IEEE, 2016.